Low-Lying Excited-States of 5-Benzyluracil

Journal:	*The Journal of Physical Chemistry*
Manuscript ID:	jp-2011-05356c.R1
Manuscript Type:	Article
Date Submitted by the Author:	n/a

Complete List of Authors:	Micciarelli, Marco; Università di Napoli Federico II, Dipartimento di Scienze Fisiche Altucci, Carlo; Università di Napoli Federico II, Dipartimento di Scienze Fisiche Bartolomeo, Ventura; Università di Napoli Federico II, Dipartimento di Scienze Fisiche Velotta, Raffaelo; Università di Napoli Federico II, Dipartimento di Scienze Fisiche Tosa, Valer; National Institute for R&D of Isotopic and Molecular Technologies, Molecular and Biomolecular Physics González Pérez, Adan; Universidade de Vigo, Departamento de Química Orgánica Pérez, Martín; Universidade de Vigo, Departamento de Química Orgánica de Lera, Angel; Universidade de Vigo, Departamento de Química Orgánica Bende, Attila; National Institute for R&D of Isotopic and Molecular Technologies, Molecular and Biomolecular Physics

Low-lying excited-states of 5-benzyluracil

Marco Micciarelli[†], Carlo Altucci[†], Bartolomeo Della Ventura[†], Raffaele Velotta[†], Valer Toşa[‡], Adán B. Gónzalez Pérez[§], Martín Pérez[§], Ángel R. de Lera[§], Attila Bende[‡,]*

[†]Dipartimento di Scienze Fisiche, Università di Napoli Federico II, via Cintia, 26-Ed. 6-80126, Napoli, Italy.

[‡]Molecular and Biomolecular Physics Department, National Institute for Research and Development of Isotopic and Molecular Technologies, Donath Street, No. 65-103, Ro-400293 Cluj-Napoca, Romania.

[§]Organic Chemistry Department, Faculty of Chemistry, Universidade de Vigo, As Lagoas - Marcosende s/n 36310, Vigo, Spain.

E-mail: bende@itim-cj.ro

[*]To whom correspondence should be addressed. Tel. +40-264-584037 ext. 194, Fax. +40-264-420042.
[†]Dipartimento di Scienze Fisiche, Università di Napoli Federico II, via Cintia, 26-Ed. 6-80126, Napoli, Italy
[‡]Molecular and Biomolecular Physics Department, National Institute for Research and Development of Isotopic and Molecular Technologies, Donath Street, No. 65-103, Ro-400293 Cluj-Napoca, Romania.
[§]Organic Chemistry Department, Faculty of Chemistry, Universidade de Vigo, As Lagoas - Marcosende s/n 36310, Vigo, Spain.

ABSTRACT: A numerical study is reported concerning the first and second singlet excited-states of 5-benzyluracil using the multireference self-consistent field (state-averaged CASSCF) method. The vertical excitation energies of low-lying excited-states were characterized using higher-level methods, such as CASPT2, MRCI, EOM-CCSD, and TDDFT. The local minima and conical intersections found on the potential energy surfaces (PESs) were characterized in terms of molecular geometry and natural population analysis. Different relaxation pathways on the PESs are identified and discussed. The molecule can be thought of as a model system for the study of crosslink reaction between DNA and proteins induced by UV light. A few suitable schemes for the crosslink process are indicated.

KEYWORDS: 5-benzyluracil; excited states; conical intersection; DNA – protein crosslinking;

1. Introduction

Short-range biomolecular interactions are crucial for sustaining all forms of life and for ensuring survival of the species through the inheritance of the genetic information. In particular, the interactions between proteins and cognate DNA are key for the replication, transcription and translation of genetic information. The analysis of gene regulation mechanisms allows decryption of the information encoded by genomes, and also can provide important tools for diagnosis, prognosis and therapy of diseases. Whereas the study of biological systems should be ideally performed without disturbing the inherent interactions (of electrostatic/polar/hydrophobic nature) between the macromolecules, in practice it is more convenient to form some stable and long-lived covalent bond (cross-linking) between the interacting bio-molecules and analyze the corresponding complexes. In particular, inducing cross-linking between nucleic acids and proteins is one of the biochemical tools for the study of the interplay between DNA and interacting proteins in living cells[1]. Stable but reversible (transient) interactions are usually induced by formaldehyde treatment before chromatin immunoprecipitation (ChIP) analysis for transcriptional studies[2]. Although this is a cheap protocol which can be run with inexpensive equipment,

it has limitations: most importantly the lack of selectivity, the long incubation times and the toxicity to cells. Alternatively, conventional UV sources[3], and nanosecond/picosecond or, more recently femtosecond ultrashort UV pulses[4,5] have been considered as alternatives to chemical cross-linking. In particular, the laser based cross-linking is very promising, since the laser can be tuned to reduce DNA damage, and to be highly specific. In addition, it could be used to probe biomolecular transient interactions in living cells.

Despite the great potential in bio-sciences, for example for genome-wide mapping of DNA-bound proteins, the knowledge of the photo-induced cross-linking mechanisms at a molecular level is scarce, and only the structures of the adducts of certain aminoacids and DNA bases (Ser-T, Cys-T, Lys-T, and Tyr-T), have so far been characterized[6-8]. In addition, the intermolecular cross-linking products of DNA bases and aminoacids are obtained in very low yields. The intramolecular version of the photo-crosslink process has recently been reported using substituted uracils, and these compounds constitute a good model system for the study of the photochemical behaviour of a particular nucleic acid base-aromatic aminoacid combination that benefit from proximity effects[9]. 5-Benzyluracil (5BU) contains a benzene ring (which replaces the aromatic part of phenylalanine) and a uracil base covalently connected through a methylene group. UV irradiation of 5BU induced a cyclization reaction and provided the bicyclic adduct in high yield, in contrast to the very inefficient intermolecular photocross-linking using mixtures of the two components[9].

We were intrigued by the efficient photochemical reaction of 5BU, and decided to theoretically study the possible singlet relaxation pathways (which are faster than those of the triplet state) that could compete with the crosslink. Being the system amenable to simulation by the use of modern computational methods, we set out to determine the molecular structure, electronic excited states energy and potential energy surface (PES) of states potentially involved in the interaction with a UV femtosecond laser pulse. In particular, this will be done for the ground state and the first two singlet excited electronic states using calculations based on geometry optimization at the multireference self-consistent field (state-averaged CASSCF) level of theory. A special care will be taken on the search of

noticeable points on the investigated PESs, i.e. local minima and conical intersections that can lead to ultrafast non-radiative decay processes. In the proximity of such points the dynamics of the process would involve more electronic states with consequent cross-talk and quantum interference between different decay paths. In addition, since the saturated methylene bridge hinders the electronic communication between components via the π systems, the description of the excited states of the uracil base is expected to contribute to the growing knowledge of the photophysical properties of substituted nucleic acid bases[10].

2. Computational Details

The geometry optimization calculations for 5BU have been performed at the state-averaged CASSCF theory level using the Molpro computational chemistry program package[11]. For this case the Dunning's double ζ + polarization (DZP) basis set[12] was taken and no symmetry restrictions were considered for the molecular geometry.

According to Matsika's and Epifanovsky's studies[13,14], if we neglect Rydberg states, the lowest excited states of the uracil fragment is originated from excitations of the valence π and lone pair n_O orbitals. Eight π and two lone pair orbitals, from the two oxygen atoms, are located on the uracil part of the molecule, thus an appropriate active space in CASSCF should include these 10 orbitals. On the other side of the molecule (the benzene fragment), there are at least six π orbitals[15], which should be included in the same active space. Therefore, in order to include in the 5BU excitation scheme these effects, the correct active space for the 5BU would be (20,16), the nomenclature (*n*,*m*) denoting here an active space of *n* electrons and *m* orbitals. This is a very large active space that results in a huge number of configuration state functions (CSFs), requiring a large amount of computational resources, even for the CASSCF level. A solution to this limitation was found by reducing CASs dimensions as described in[14] for pure uracil where (14,10) and (12,9) CASs have been tested. We have found that for 5BU the best compromise solution was not the extension on the two-ring molecule of the reduced CASs used in[13], but the (20,14), corresponding to the exclusion of the highest unoccupied orbital from the active space. This

choice drastically reduces the number of CSFs causing just some convergence problems in the MCSCF cycles. For the (20,14) active space, the number of CSFs generated is 273,273, while the number of determinants is 1,002,001. In order to estimate the role of virtual orbitals in the excitation energy calculation we have used also the (20,15) CAS to compute the vertical excitation energy. Here a number of 1,002,001 CSFs and 4,008,004 determinants were obtained.

In order to take into account the effect of electron correlations (static and dynamic) for the vertical excitation energies evaluation, we have performed further calculations using higher-level methods: (i) multireference configuration interaction (MRCI)[16] with and without Davidson (D) correction[17], (ii) multi state second-order multireference perturbation theory (MS-CASPT2)[18], (iii) equation-of-motion coupled-cluster theory for excited states (EOM-CCSD)[19-21], (iv) and the time-dependent density functional theory (TDDFT)[22,23]. For MRCI, MS-CASPT2 and EOM-CCSD cases we used Molpro software while for TDDFT, Gaussian03[24] package was employed. In case of MS-CASPT2 calculations a level shift[25,26] parameter of 0.2 was considered. For all multireference and the single-reference CC2[27] methods the first two electronic singlet excited states, S_1 and S_2, were accounted for. In case of CC2 method the Laplace Transformed Local CC2 version (LT-DF-LCC2)[28-30] with Density-Fitting[31-33] approximation was used together with the cc-pVTZ auxiliary basis set[34,35] (*JKFIT* and *MP2FIT*).

Unfortunately, the use of multireference methods including dynamic electron correlation exceeds our computer capacity for geometry optimization purposes. Therefore, all geometry optimizations were performed at the SA-CASSCF level. Our challenging (20,14) active space was only used for MS-CASPT2 and a single point energy calculation. For this reason we were forced to reduce once more the dimension of our active space from (20,14) to (20,13) keeping only four virtual orbitals. With the (20,13) active space we succeeded in computing also the MRCI energies. The 5BU system contains 106 electrons with 53 double occupied orbitals. In the case of geometry optimizations, by using the SA-MCSCF method, we kept the first 43 orbitals closed, which means that these orbitals were doubly occupied in all CSFs, but they were fully optimized during the MCSCF cycle. On the other hand, for the

vertical excitation energies calculation with methods including the electron correlation evaluation, all 43 orbitals, which were not included in the active space, were kept frozen.

Finally, for all geometries the natural population analysis (NPA)[36,37] was included along with the Wiberg's bond-order index (BI)[38] implemented in the Molpro package. Molecular structures were visualized and analyzed using the Gabedit[39] molecular graphics program, while the molecular graphics (figures) were created using the Avogadro[40] software.

3. Results and Discussion

3.1 Vertical and Adiabatic Excitation Energies. As we already mentioned in the previous section, the *ground state* optimized geometrical structure of 5BU was obtained using the SA-MCSCF method with DZP basis set, considering the (20,15) active space configuration. Its geometry is shown in **Figure 1**, where "ring atoms" have been denoted with numbers (*1*…*6*) and with letters (*a*…*f*) for uracil and benzene, respectively. As one can observe from **Figure 1** the optimized ground state geometry of 5BU presents two planar structures defined by the uracil and benzene rings where the planes between them form an angle of 113.8°. In the following the geometries will be denoted by $R_e^{Xi}(S_Y)$, where Xi = Bi or Ui (B= benzene, U= uracil) is used to differentiate stationary points on uracil or benzene branches, Y = 0, 1 or 2 is to show the order of the given excited state related to the energy quantum number, while *e* indicate the nature of the stationary point (equilibrium geometry or not). The bond lengths and bond indexes of the $R_e(S_0)$ geometry are presented in **Table 1** (second and third columns, respectively). The geometry parameters of the uracil fragment are quite close to the values obtained by Matsika[13] for isolated uracil, while the benzene ring loses its symmetry. The C-C bond lengths are not anymore equal but differ by about 0.005 Å. Based on the Wiberg BI analysis, one can see that the uracil fragment contains three "double bonds" with the BI ≈ 1.6, while other bonds are classical single bonds with BI ≈ 1.0. With regards to the benzene ring, the BI varies between 1.24 – 1.30 showing a slight deviation from its value[41] in the perfect aromatic ring.

The vertical excitation energies up to the second excited level are presented in **Table 2**, as calculated with different methods. The results for the first excited (S_1) state are in a reasonably good agreement with each other except for TDDFT result. This last result was obtained with the B3LYP[42-44] exchange-correlation (XC) functional and slightly underestimates the energy value. For the second excited state (S_2) this picture is not simple anymore. While the multireference methods give values higher than 6.8 eV, single reference methods are close to S_1 vertical excitation energy. The explanation of this discrepancy could be related to the inability of these methods to properly describe the σ – π polarization effects[45] due to the limitations on the number of virtual orbitals involved in the multiconfiguration wavefunction. This kind of discrepancy is extensively investigated in ref 14, where a special MRCI method is introduced, called MRCIσπ, in which all the single excitations for the σ electrons in the valence *n,π* space are allowed except for the 1s core orbitals. In this way the energy value for the second excited state of the simple uracil molecule has been found to be 0.5 eV lower than that obtained by means of the ordinary MRCI. In order to be able to estimate the effect of virtual orbitals cut off, we have performed MS-CASPT2 single point energy calculation using the (20,14) active space. The S_2 vertical excitation energy was substantially improved, we obtained 6.28 eV, which is 0.55 eV smaller than similar value computed with the (20,13) active space. On the other hand, a more recent work on the uracil system[14,46] emphasized that the use of high-quality basis sets with diffuse functions (i.e., aug-cc-pVTZ or aug-ANODZ) is important for obtaining a good agreement with the experimental values. However, as the 5BU is structurally more complex, a calculation with this high-quality basis set is, unfortunately, not yet feasible.

A critical issue for the laser-induced excitation of a molecule is to find, for the excited states, different stationary points on the PESs and possible intersections between different PESs. The detailed characterization and discussion of these crossing points, i.e., conical intersection, is given below.

The geometry optimization of the first and second excited states was first performed starting from the optimized geometry of the ground state. For both states the resultant forces induce geometry changes only at the benzene side. For the S_1 state a stationary point characterized by the $R_e^B(S_1)$ geometry was

found. Compared to the $R_e(S_0)$ geometry, the benzene ring's C-C bonds become longer in average by 0.038 Å and their BI-s become closer to each other. At the same time, no geometry change can be found at the uracil branch for the $R_e^B(S_1)$ geometry. The energy of this $R_e^B(S_1)$ stationary point falls 4.63 eV above the ground state energy level, which is always set as the zero-point of the energy scale in this work. In order to find other stationary points on the PES of S_1 state where the uracil fragment is involved, we have slightly modified the starting geometry by stretching the C^4=O double bond. In this way the resultant forces during the geometry optimization induce changes in the uracil fragment. This stationary point is characterized by the $R_e^U(S_1)$ geometry and its molecular graphics is shown in **Figure 2**. In this 5BU structure the uracil fragment shows a non-planar geometry, where hydrogen atoms bound to the N^3 nitrogen as well as to the C^6 carbon atoms moved out from the molecular plane of the uracil fragment. Furthermore, the C^4=O double bond stretches from ≈ 1.2 Å to ≈ 1.4 Å, the C^4-C^5 bond becomes shorter (from ≈ 1.5 Å to ≈ 1.4 Å), and the C^5-C^6 bond becomes longer (from 1.35 Å to 1.41 Å). These changes are also reflected in the BI values. The C^4-C^5 bond switches from a single bond (BI=1.03) in the ground state to a stronger one with BI=1.37, while the C^5-C^6, initially a "double bond" (with BI=1.66), here changes to a weaker bond (with BI=1.24). Likewise the C^4=O "double bond" (with BI=1.62) turns onto a "single bond" (with BI=1.16). On the benzene side this geometry changes are more moderate, in the order of few percent or lower for the bond lengths. At the same time, the benzene ring is rotated by 26.7° compared to its position in the ground state. The reference energy of this $R_e^{U1}(S_1)$ stationary point is 4.19 eV being 0.44 eV lower than the stationary point energy of the $R_e^B(S_1)$ geometry. Another stable geometry of $R_e^{U1}(S_1)$, labeled $R_e^{U2}(S_1)$, was found on the S_1 PES (See **Figure 3**). The reference energy of this $R_e^{U2}(S_1)$ stationary point is 4.72 eV. This $R_e^{U2}(S_1)$ geometry can easily turn over to the $R_e^{U1}(S_1)$ geometry by internal vibrational relaxation, because the two geometries are symmetric with respect to the uracil plane.

When studying the S_2 geometry relaxation starting from the optimized ground state, the changes occur again on the benzene side. Nevertheless we did not find any stationary point before reaching a conical

intersection between the S_1 and S_2 PESs. Using the same procedure of inducing a stretch in the C^4=O double bond we found two different stationary points corresponding to the $R_e^{U1}(S_2)$ and $R_e^{U2}(S_2)$ configurations.

The $R_e^{U1}(S_2)$ geometry is shown in **Figure 4**. Similarly to $R_e^{U1}(S_1)$, the geometry distortion is noticed predominantly in the uracil fragment, but, unlike the S_1 configuration, different bonds in uracil are affected. In particular, the most conspicuous difference is observed in the relative position of the C^6-H bond, where the movement of the H atom away from the molecular plane is larger than in the S_1 case, while the deviation of the H atom from the N^3-H bond is barely observed. Furthermore, the C^5-C^6 bond is more elongated (from 1.41 Å to 1.49 Å) and shows features of a "single bond" (with BI=1.15), while the C^4-C^5 bond becomes shorter and presents a more characteristic "double bond" nature (with BI=1.41). In this case, the benzene ring is rotated by 20.9° from its position in the ground state geometry, and the reference energy of this $R_e^{U1}(S_2)$ stationary point is 5.99 eV.

The next stationary point found in the S_2 surface is defined by the $R_e^{U2}(S_2)$ geometry depicted in **Figure 5**. Here, the major deformation consists in the deviation from the uracil molecular plane and the extension of the C^4=O double bond which turns onto a single bond (BI=0.83). The other bond distances are slightly modified, with the C^4-C^5 and C^5-C^6 bonds keeping their properties as in the ground state. On the other hand, for this $R_e^{U2}(S_2)$ geometry the benzene ring is rotated only by 5.9° from its position in the ground state. The reference energy of this $R_e^{U2}(S_2)$ stationary point is 6.46 eV, being 0.47 eV higher than the stationary point energy of the $R_e^{U1}(S_2)$ geometry.

3.2 Crossing points. As mentioned in the previous subsection, in the case of the S_2 PES, no stationary points were found with modified coordinates on the benzene branch. The geometry optimization led us directly to conical intersection (CI) points between the S_1 and S_2 PESs. These structures are defined by the $R_{CI}^{B1}(S_1S_2)$ and $R_{CI}^{B2}(S_1S_2)$ geometries with the important bond distances listed in **Table 3**, and their molecular graphics presented in Supporting Information (**Figure S1** and **Figure S2**). The benzene ring distortion is very close to the configuration of S_1 and S_2 conical intersection point obtained by Robb[15]

for the individual benzene molecule, while the uracil fragment remains almost unchanged. The planar structure of the benzene ring is broken, the C^e carbon atom moving away from the molecular plane and forming two "single bonds" with the C^d and C^f atoms. The reference energy of this $R_{CI}^{B1}(S_1S_2)$ conical intersection point is 6.49 eV, while the in case of $R_{CI}^{B2}(S_1S_2)$ this reference energy is 6.50 eV.

Starting from the $R_e^{U1}(S_2)$ and $R_e^{U2}(S_2)$ geometries, two different CI points, labeled $R_{CI}^{U1}(S_1S_2)$ and $R_{CI}^{U2}(S_1S_2)$, were found at the uracil side. Their geometry parameters are presented in **Table 3a**, and their graphics are shown in the Supporting Information (**Figures S3** and **S4**). In both cases the uracil fragment is distorted. The $R_{CI}^{U1}(S_1S_2)$ geometry is quite similar to the CI geometry of the individual uracil molecule obtained in ref 12. In both conical intersection geometries, the most affected atoms are C^4, C^5 and C^6, as well as the C^4=O bond. In the first case, $R_{CI}^{U1}(S_1S_2)$, the uracil ring planarity is broken, adopting a "V" shape, while in the second CI geometry, $R_{CI}^{U2}(S_1S_2)$, the ring planarity is maintained, but the H atom from the N^3-H bond gets closer to the O atom of C^4=O bond. In this way two intermediate bonds, N^3-H-O with BI(N^3-H)=0.39 and BI(O-H)=0.27 are formed. The reference energies for these S1-S2 conical intersection structures are 5.50 eV for $R_{CI}^{U1}(S_1S_2)$ and 7.74 eV for $R_{CI}^{U2}(S_1S_2)$. Here, one should mention that the second CI point is located at a relatively high energy level and it is difficult to reach during the geometry relaxation processes.

Besides the S1-S2 conical intersection points, the S0-S1 CIs are also very important. Accordingly, we carried out further search of CIs starting from the geometry structure of the S_1 minima, both at the benzene and at the uracil fragments. In this case, two other CI crossing points, namely $R_{CI}^{B}(S_0S_1)$ and $R_{CI}^{U}(S_0S_1)$, were found, the former showing deformation of the benzene ring and the latter distortion of the uracil ring. Their geometries are presented in the Supporting Information (**Figures S5** and **S6**), while the corresponding bond values and indexes are given in **Table 3b**. For the $R_{CI}^{B}(S_0S_1)$ CI structure the benzene ring bends along the C^1 and C^5 carbon atoms (resembling a fulvene structure), the aromatic character is partially lost and the C-C bond strengths change. Accordingly, the C^3 atom forms two partial double bonds (with BIs close to 1.45) with its C^2 and C^4 neighbouring carbon atoms and a classical C-H

bond as well. The reference energy of this $R_{CI}^{B}(S_0S_1)$ structure is 4.68 eV. With regard to the $R_{CI}^{U}(S_0S_1)$ CI structure, mainly the uracil fragment is distorted whereas the C-C bonds from the benzene fragment show very small deviations from the C-C bond distances found in the $R_e(S_0)$ geometry. In the uracil fragment, again, a single-to-double bond transition can be observed when compared with the ground state optimized geometry, which is most clearly apparent by following the BIs. Namely, the BI of C^4-C^5 changes from 1.03 to 1.44 becoming a double bond and simultaneously the BI of C^5-C^6 changes from 1.66 to 1.04 forming a single bond; also the C^4-O double bond turns into a single bond. The reference energy of this $R_{CI}^{U}(S_0S_1)$ CI structure is 4.60 eV.

3.3 Relaxation pathways. In molecules with high symmetry, the location of the CI points depends on the symmetry properties of these molecules. Nowadays it is widely accepted that even in the case of low-symmetry molecular systems the CIs – called accidental CIs[47] – are much more common than previously thought and these CIs play a crucial role in nonadiabatic events (e.g., radiationless decay of electronic excited states)[48-51]. However, knowing only the location of the CI points and energy minima on the PESs is not sufficient to draw a realistic picture about the relaxation mechanism of the molecular excited states. This is because several potential energy barriers, smaller or higher, can occur on the PES between energy minima and CI points and thus obstruct reaching these critical points. On the other hand, the time scale of these relaxation mechanisms can be correctly evaluated only after a thorough molecular dynamics study of these nonadiabatic processes. This would require the use of more demanding computational methods that can reproduce correctly the dynamics near the CI points[52-54]. In this section, our aim is not to give an exhaustive description of the relaxation dynamics of 5BU, but to estimate possible pathways for different geometrical transitions and to draw a qualitative picture about the relaxation mechanisms of the molecule excited states. Finding an energy minimum on the PES is relatively straightforward because the negative of the gradient always points downhill. By contrast, a transition structure (TS) optimization must step uphill in one direction and downhill in all other orthogonal directions and therefore requires special searching methods[55] including a preliminary evaluation of the Hessian matrices for each case. In order to draw a qualitative picture about the crossing

between different critical points on the PESs we have applied the linear synchronous transit (LST)[56] method (the first step of the QST2[57] method), which gives the direct crossing line between two different points on the surface but with much less computational effort than other TS searching methods. Unfortunately, in this way we could find only second order saddle-points and not the real TS geometries.

The first energy gap analyzed was the linear transition between the vertical $R_e(S_0)$ (which characterize also the vertical S_1 and S_2 states) and the $R_e^{U1}(S_2)$ optimized geometries. The profile of this energy gap is shown on **Figure S7** (Supporting Information). The very large energy barriers (over 19.0 eV) for both S_1 and S_2 excited states make unlikely the transitions between vertical and optimized geometries at the S_2 electronic level. This explains why optimized geometries on the uracil branch could only be obtained starting from a geometry with forced stretching of the C=O bond. On the descending part of the graph the S_1 (red) and S_2 (blue) states get quite close to each other. Starting from this 5BU geometry we have performed a new CI search in order to check whether or not these two states cross each other. Only an avoided crossing point was found with a 0.018 eV (0.418 kcal/mol) energy gap between the S_1 and S_2 states. The geometry of this avoided crossing point is shown in the Supporting Information (**Figure S8**). Similarly, very large energy barriers were obtained between the vertical $R_e(S_0)$ and the $R_e^{U}(S_1)$ optimized geometries. The profile of the energy gap, shown in the Supporting Information (**Figure S9**), has similar features described for the linear transition between the vertical $R_e(S_0)$ and the $R_e^{U1}(S_2)$ optimized geometries (**Figure S7**, Supporting Information).

The transition between the vertical $R_e(S_0)$ and the $R_e^{U2}(S_2)$ optimized geometries is depicted in the Supporting Information (**Figure S10**). This LST show a more interesting picture of the relaxation mechanism with much lower energy barriers involved. The S_2 state starts with a strong decrease, while the S_1 slightly increases, then, they cross each other after four geometry steps. After this crossing point the S_2 state transits a relatively small energy gap (~1.6 eV), while the S_1 state will reach the $R_e^{U2}(S_1)$ optimized geometry. In order to find out the nature of the crossing point, which occurs between the S_1 and S_2 states after a few LST steps, we have started a new CI point search taking as starting structure

this LST step geometry. We found an avoided crossing point (instead of CI point) with an energy barrier of 0.0043 eV (0.1 kcal/mol). Its geometry is presented as Supporting Information (**Figure S11**). The energy barriers indicate that a more feasible relaxation is obtained by displacing the oxygen atom of the C^4=O bond out from the uracil molecular plane (**Figure S10**, Supporting Information) rather than by stretching the C^4=O bond in the molecular plane (**Figure S7**, Supporting Information).

As we mentioned in subsection 3.2, there is no any energy barrier between the vertical $R_e(S_0)$ and an optimized geometry structure of the S_2 state at the benzene branch, because we directly reach one of the $R_{CI}^{B1}(S_1S_2)$ or $R_{CI}^{B2}(S_1S_2)$ CI points. The transit between the vertical $R_e(S_0)$ and the optimized geometry structure of S_1 state $R_e^B(S_1)$ follows a slightly descending potential curve without any energy barrier (**Figure S12**, Supporting Information).

We computed also the LST between the two S_1 optimized geometries found at the uracil ($R_e^{U1}(S_1)$) and benzene ($R_e^B(S_1)$) branches. We found the same behavior as in the case of the $R_e(S_0)$ – $R_e^{U1}(S_2)$ transit, with a very large (more than 20 eV) potential barrier (see **Figure S13**, Supporting Information).

The LST trajectories between different optimized and CI geometries were also analyzed (Figure S14, Supporting Information). The LST between the $R_e^{U1}(S_2)$ optimized geometry and the $R_{CI}^{U1}(S_1S_2)$ conical intersection point reveals two potential barriers, each around 2.0 eV. According to the prediction of Barbatti *et al.*[58] for the case of the non-adiabatic deactivation of 9H-adenine, a time scale of 100 – 120 fs would be required to surpass a 1.5 - 2 eV energy barrier. Therefore we surmise that the transit from the $R_e^{U1}(S_2)$ optimized geometry to the $R_{CI}^{U1}(S_1S_2)$ conical intersection point could take place in a reasonable time scale. It was also shown[58] that radiationless deactivation among higher excited states can occur very fast through CIs. The slowest transition is considered to be the deactivation process between the first excited and the ground state. Accordingly, we have investigated both S_1 – S_0 transitions in the uracil (See **Figure S15**, Supporting Information) and benzene (See **Figure S16**, Supporting Information) fragments. The energy barriers along the LST trajectories were found to be 2.76 eV and 4.03 eV for uracil and benzene, respectively. Although both barriers are high enough to partially prevent the non-

adiabatic decays, these values suggest that a radiationless deactivation to the ground state would more easily occur in the uracil than in the benzene sides and that the radiative transition is an alternative mechanism to reach the ground state. This was experimentally confirmed by us and is analyzed in the next subsection.

3.4. Fluorescence measurements and comparison with theoretical predictions. We have measured the static fluorescence spectrum of 5BU in methanol when excited with UV radiation, at 247 nm (5 eV) and 265 nm (4.7 eV), respectively. These two wavelengths virtually cover the whole range of vertical excitation energies as calculated through several different methods (see Table 2). We notice that EOM-CCSD, LT-DF-LCC2 and TDDFT (B3LYP) methods predict even vertical excitation of the second excited states, S_2, thus accessing more complicated decay paths. In fact, from S_2 the molecule can reach the S_1 state and reach a conical intersection with a radiationless decay to the ground state or populate the $R_e^{U1}(S_1)$ and the $R_e^{B}(S_1)$ states, decaying to the ground by emission of a photon.

The measurements have been carried out with a LS 55 fluorescence spectrophotometer (PerkinElmer) in samples having a concentration of 0.01 M and led to the results shown in **Figure 6**, where both solid and dashed spectra have been represented using the same y-axis allow comparison of the spectral amplitudes in the two cases. Two fluorescence bands are observed at about 315 nm (3.9 eV), and 365 nm (3.4 eV). While the position of the peaks is not substantially shifted when switching from 247 nm to 265 nm excitation wavelength, the ratio of the two peak amplitude, A_{315}/A_{365}, changes from about 1:0.95 to about 0.9:1. Based on the scheme of the energy levels illustrated in **Figure 7**, we ascribe the two fluorescence bands to radiative decay from the $R_e^{B}(S_1)$ state for the 315-nm peak and from the $R_e^{U1}(S_1)$ state for the 365-nm peak, respectively.

In order to test the reliability of our interpretation we have checked that the two states $R_e^{B}(S_1)$ and $R_e^{U1}(S_1)$ can be actually reached while the molecules are relaxing after excitation. This issue is solved by exhibiting at least one allowed decay path leading to $R_e^{B}(S_1)$, represented in **Figure 7**, which shows a possible relaxation from a vertical excitation to the S_1 PES down to $R_e^{B}(S_1)$. Another possible decay path

leading to $R_e^{U1}(S_1)$, and represented in **Figure 7**, shows a possible relaxation from a vertically excited S_2 PES down to $R_e^{U1}(S_1)$ via a conical intersection. The measured UV-fluorescence spectrum of uracil in methanol solution[59] shows a peak around 315 nm with a shoulder at about 365 nm. Based on our calculations we could conclude that the presence of the benzene ring in the bridged 5BU molecule leads to a consistent enhancement of the shoulder at 365 nm. This hypothesis has a very important consequence in that we can actually distinguish the fluorescence from the molecules excited in the benzene site from the fluorescence emitted by the molecules excited in the uracil site. It is worth mentioning that, in order to carry out a fair comparison between theory and experiment, we specifically calculated the energy gap between the excited states, $R_e^B(S_1)$ and $R_e^{U1}(S_1)$, and the ground state, $R(S_0)$, respectively, for a vertical decay, i.e. when the nuclei of $R(S_0)$ are found in the $R_e^B(S_1)$ and $R_e^{U1}(S_1)$ configuration, respectively. Such energy gaps are found to be 4.46 eV for the $R_e^B(S_1) \rightarrow R_e(S_0)$ transition and 3.36 eV for the $R_e^{U1}(S_1) \rightarrow R^U(S_0)$ transition. Interestingly, for the $R_e^B(S_1) \rightarrow R^B(S_0)$ transition, the calculated energy gap overestimates by 0.6 eV the corresponding measured value, whereas for the $R_e^{U1}(S_1) \rightarrow R^U(S_0)$ transition the calculation is very close to the corresponding experimental value. The 0.6 eV discrepancy can be ascribed to the correction of the real energy level in solution due to the presence of a polar solvent. Indeed, it has been shown by Improta *et al*[60] that the energy of the fluorescence photon increases in solution in comparison to the gas phase when n/π* transitions are involved, whereas it lowers for π/π* transitions. Since the transitions are n/π* for the uracil branch and π/π* for the benzene branch the observed shifts are in good agreement with those predicted by Improta *et al.*[60], thus supporting our results.

4. Summary and Conclusions

We have investigated the decay paths located on the first and second singlet excited-state surfaces of 5BU, a molecule which attracts a noticeable interest as it is considered as a model system for the study of nucleic acid-protein crosslink reactions induced by UV light. The structures found for the benzene

and uracil fragments in 5BU, as seen in **Figure 1**, are close to the ones already obtained for the isolated compounds[13,15] in the electronic ground state, except for the benzene symmetry breaking. Therefore, the CH_2 bridge behaves just as a small perturbation giving rise to minor changes in molecular structure, and this supports the idea that 5BU can be actually used as model system for the photo-crosslink reaction.[9]

The first two electronic excited states in the $R_e(S_0)$ nuclear geometry have been characterized with both multireference and single determinant methods. The results are in a reasonably good agreement for the S_1 state, and only TDDFT method underestimates slightly the energy value. For the S_2 state, multireference methods give values higher than 6.8 eV, whereas those obtained with single reference methods are close to the S_1 vertical excitation energy. This is likely due to the fact that not all the needed orbitals in the active space could be included for the CASSCF method to properly work. On the other hand, it is well known that single determinant methods are not able to properly describe the static correlation due to the degeneracy of electronic states. The relatively small energy difference between the first and second excited states obtained either with coupled-cluster or DFT theories suggest that one should not totally ignore the effect of static electron correlation.

The geometry optimizations on the S_1 PES, starting from the nuclear geometry $R_e(S_0)$, did not lead to significant changes on the uracil branch of the molecule. On the S_1 PES, just the C^4=O double bond stretching, involved in several vibrational modes, led to the $R_e^{U1}(S_1)$ geometry (**Figure 2**), where the uracil fragment shows a non-planar geometry. The geometry optimizations on the S_2 PES, when started from the nuclear geometry $R_e(S_0)$ led to a conical intersection point with the S_1 PES with a subsequent relaxation of the system on this surface. The same procedure of C^4=O double bond stretching led us to find two other minima on this surface, the $R_e^{U1}(S_2)$ (**Figure 4**) which exhibits the same or even accentuated reactivity as $R_e^{U1}(S_1)$, and the $R_e^{U2}(S_2)$ (**Figure 5**), which is less reactive.

We have also found three conical intersections that could play a crucial role in the 5BU decay pathways: as for the single isolated fragments - benzene and uracil -, they represent ultrafast non-radiative decay channels leading to lower energy electronic states. These have been characterized as (i)

$R_{CI}^{B1}(S_1S_2)$ (**Figure S1**, Supporting Information), in which the uracil fragment is close to the ground state $R_e(S_0)$ geometry and the benzene fragment structure is close to that found by Robb[15]; (ii) the $R_{CI}^{U1}(S_1S_2)$ (**Figure S3**, Supporting Information), for which the uracil fragment is close to the conical intersection found by Epifanovsky *et al*[14]; and (iii) the $R_{CI}^{U2}(S_1S_2)$ (**Figure S4**, Supporting Information).

A global picture with different relaxation pathways defined by local minima and conical intersection points on the PES-s is presented in **Figure 7**. Red dashed lines show the less feasible paths, while the blue ones give the more plausible transitions. The radiation-type transitions are marked with arrow lines. An approach to the deactivation pathway that can undergo 5BU is depicted from the S_1 and the S_2 states, respectively. The most likely pathways that the molecule would follow when the excitation leads to the S_2 excited state is the vibrational decay to the $R_e^{U2}(S_2)$ geometry that would evolve through the $R_{CI}^{U1}(S_1S_2)$ conical intersection to the S_1 PES relaxing vibrationally to the $R_e^{U1}(S_1)$. Finally the system could energetically reach the $R_{CI}^{U1}(S_0S_1)$ leading the electronic state of the molecule to the minima in the ground state initial geometry or directly via radiation decay from $R_e^{U1}(S_1)$ to $R_e(S_0)$. Other possible pathways via the benzene branch starts from S_2 state and reach the S_1 state following either the $S_2 \rightarrow R_{CI}^{B1}(S_1S_2)$ or $R_{CI}^{B2}(S_1S_2) \rightarrow R_e^{B}(S_1)$ radiationless decays. Eventually the non-radiative $R_e^{B}(S_1) \rightarrow R_{CI}^{B}(S_0S_1) \rightarrow R_e(S_0)$ relaxations or the corresponding direct radiative transitions can take the molecule to S_0 state.

This work represents a first step in the characterization of the nucleic acid-proteins crosslink reaction at the molecular level using *ab initio* methods. A natural extension of the static knowledge about the 5BU molecular system, which we provided with this theoretical investigation, will include solvent (for a condensed phase simulation) and thermal effects. As a near-future prospect we plan to apply the *ab initio* molecular dynamics approach to investigate the system dynamics, and use the above calculations as a reference for the planned molecular dynamics calculations.

ACKNOWLEDGMENT. This work has been supported by the European Union (FP7, Health-F4-2009-221952; ATLAS). We gratefully acknowledge for providing computational infrastructure and the

technical assistance of the Data Center of NIRDIMT Cluj-Napoca. (A.B.) thanks to Dr. Richardo Mata for providing a special NBO source code for the Molpro program package. (A.B.) is also thankful for the Grant of European Science Foundation (Ref. No. 3367/2010) supporting his visit at the Faculty of Chemistry, University of Vigo (Spain).

References and Notes

(1) Sperling, R.; Havron, A.; Sperling, J. *Ann. N. Y. Acad. Sci.* **1980**, *346*, 386.

(2) Solomon, M. J.; Larsen, P.L.; Varshavsky, A. *Cell* **1988**, *53*, 937.

(3) Zhang, L.; Zhang, K.; Prändl, R.; Schöffl, F. *Biochem. Biophys. Res. Commun.* **2004**, *322*, 705.

(4) Russmann, Ch.; Truss, M.; Fix, A.; Naumer, C.; Herrmann, T.; Schmitt, J.; Stollhof, J.; Beigang, R.; Beato, M. *Nucl. Acids Res.* **1997**, *25*, 2478.

(5) Russmann, Ch.; Beato, M.; Stollhof, J.; Weiss, C.; Beigang, R. *Nucl. Acids Res.* **1998**, *26*, 3967.

(6) Wang, W. Y. *Photochemistry and Photobiology of the Nucleic Acids*; Wiley: New York, 1976.

(7) Morrison, H. *Bioorganic Photochemistry*, Wiley: New York, 1990.

(8) Shetlar, M. D. In *Frontiers of Photobiology,* Proceedings of the 11th International Congress on Photobiology, Kyoto, Japan, 7-12 September 1992 (International Congress Series); Shima, A., Ichihashi M. Eds.; Excerpta Medica 1993, Vol. 1021, pp 67.

(9) Sun, G.; Fecko, C.; Nicewonger, R. B.; Webb W. W.; Begley, T. P. *Org. Lett.* **2006**, *8*, 681.

(10) Bányász, Á.; Karpati, Sz.; Mercier, Y.; Reguero, M.; Gustavsson, T.; Markovitsi, D.; Improta, R. *J. Chem. Phys. B*, **2010**, *114* 12708.

(11) MOLPRO, version 2009.1, A package of *ab initio* programs, Werner, H.-J.; Knowles, P. J. Lindh, R.; Manby, F. R.; Schütz, M.; Celani, P.; Korona, T.; Mitrushenkov, A.; Rauhut, G.; Adler, T. B.; *et al.* see http://www.molpro.net.

(12) Dunning Jr, T. H.; Hay, P. J. In *Modern Theoretical Chemistry*; Schaefer III, H.F. Eds.; Plenum: New York, 1976; Vol 3. pp 1–28.

(13) Matsika, S. *J. Phys. Chem. A* **2004**, *108*, 7584.

(14) Epifanovsky, E.; Kowalski, K.; Fan, P.-D.; Valiev, M.; Matsika, S.; Krylov, A. I. *J. Phys. Chem. A* **2008**, *112*, 9983.

(15) Palmer, I. J.; Ragazos, I. N.; Bernardi, F.; Olivucci, M.; Robb, M. A. *J. Am. Chem. Soc.* **1993**, *115*, 673.

(16) Knowles, P. J.; Werner, H.-J. *Theor. Chim. Acta* **1992**, *84*, 95.

(17) Langhoff, S. R.; Davidson, E. R. *Int. J. Quant. Chem.* **1974**, *8*, 61.

(18) Celani, P.; Werner, H.-J. *J. Chem. Phys.* **2000**, *112*, 5546.

(19) Monkhorst, H. J. *Int. J. Quantum Chem. Symp.*, **1977**, *11*, 421.

(20) Stanton; J. F., Bartlett, R. J. *J. Chem. Phys.*, **1993**, *98*, 7029.

(21) Korona, T.; Werner, H.-J. *J. Chem. Phys.* **2003**, *118*, 3006.

(22) Runge, E.; Gross; E. K. U. *Phys. Rev. Lett.*, **1984**, *52*(12), 997.

(23) Stratmann, R. E.; Scuseria, G. E.; Frisch, M. J. *J. Chem. Phys.*, 1998, *109*, 8218.

(24) Gaussian 03, Revision C.02, Frisch, M. J.; Trucks, G. W.; Schlegel, H. B.; Scuseria, G. E. Robb, M. A.; Cheeseman, J. R.; Montgomery Jr., J. A.; Vreven, T.; Kudin, K. N.; Burant, J. C.; *et al.* Gaussian, Inc., Wallingford CT, 2004.

(25) Lorentzon, J.; Fulscher, M. P.; Roos, B. O. *J. Am. Chem. Soc.* **1995**, *117*, 9265.

(26) Roos, B. O.; Andersson, K. *Chem. Phys. Lett.* **1995**, *245*, 215.

(27) Christiansen, O.; Koch, H.; Jørgensen, P. *Chem. Phys. Lett.*, **1995**, *243*, 409.

(28) Kats, D.; Korona, T.; Schütz, M. J. Chem. Phys., **2006**, *125*, 104106.

(29) Kats, D.; Korona, T.; Schütz, M. J. Chem. Phys., **2007**, *127*, 064107.

(30) Kats, D.; Korona, T.; Schütz, M. J. Chem. Phys., **2009**, *131*, 124117.

(31) Vahtras, O.; J. Almlöf, J.; Feyereisen, M. V. *Chem. Phys. Lett.*, **1993**, *213*, 514.

(32) Schütz, M. *J. Chem. Phys.*, **2000**, *113*, 9986.

(33) Schütz, M.; Werner, H.-J. *J. Chem. Phys.*, **2001**, *114*, 661.

(34) Weigend, F.; Köhn, A.; Hättig, C. *J. Chem. Phys.*, **2002**, *116*, 3175.

(35) Weigend, F. *PhysChemChemPhys*, **2002**, *4*, 4285.

(36) Foster, J. P.; Weinhold, F. *J. Am. Chem. Soc.* **1980**, *102*, 7211.

(37) Reed, A. E.; Weinstock, R. B.; Weinhold, F. *J. Chem. Phys.* **1985**, *83*, 735.

(38) Wiberg, K. A. *Tetrahedron* **1968**, *24*, 1083.

(39) Allouche, A. R. *J. Comput. Chem.* **2010**, *32*, 174.

(40) Avogadro: an open-source molecular builder and visualization tool. Version 1.1, http://avogadro.openmolecules.net/

(41) Xu, S.; Wang, C.; Cui, Y. *Chin. J. Chem.* **2010**, *28*, 734.

(42) Becke, A. D. *Phys. Rev. A*, **1988**, *38(6)*, 3098.

(43) Lee, C.; Yang, W.; Parr R. G. *Phys. Rev. B*, **1988**, *37(2)*, 785.

(44) Vosko, S. H.; Wilk, L.; Nusair, M. *Can. J. Phys.* **1980**, *58(8),* 1200.

(45) Borden, W. T.; Davidson, E. R. *Acc. Chem. Res.* **1996**, *29*, 67.

(46) Fleig, T.; Knecht, S.; Hättig, C. *J. Phys. Chem. A*, **2007**, *111*, 5482.

(47) Matsika, S.; Yarkony, D.R. *J. Chem. Phys.* **2002**, *117*, 6907

(48) Bernardi, F.; Olivucci, M.; Robb, M. A. *Chem. Soc. Rev.* **1996**, *25*, 321.

(49) Yarkony, D.R. *J. Phys. Chem. A* **2001**, *105*, 6277.

(50) Domcke, W.; Yarkony, D.R.; Köppel, H. *Conical Intersections: Electronic Structure, Dynamics and Spectroscopy*. Singapore: World Sci. 2004.

(51) Matsika, S.; Krause, P. *Annu. Rev. Phys. Chem.* **2011**, *62*, 621.

(52) Meyer, H.D.; Mante, U.; Cederbaum, L.S. *Chem. Phys. Lett.* **1990**, *165*, 73.

(53) Tully, J.C. *Faraday Discuss.* **1998**, *110*, 407.

(54) Doltsinis, N. L.; Marx, D. *J. Theor. Comput. Chem.* **2002**, *1*, 319.

(55) Schlegel, H.B. *WIREs Comput. Mol. Sci.* **2011**, **1**, 790.

(56) Halgren, T.; Lipscomb, W.N. *Chem. Phys. Lett.* **1977**, *49*, 225.

(57) Peng, C.Y.; Schlegel, H.B. *Isr. J. Chem.* **1993**, *33*, 449.

(58) Barbatti, M.; Lischka, H. *J. Am. Chem. Soc.* **2008**, *130*, 6831.

(59) Gustavsson, Th.; Sarkar, N.; Bányász, Á.; Markovistsi, D.; Improta, R. *Photochem. Photobiol.* **2007**, *83*, 595.

(60) Improta, R; Barone, V. *J. Am. Chem. Soc.*, **2004**, *126*, 14320.

Table 1. Internal Bond Coordinates and the Wiberg's bond index (BI) of the Optimized Geometries at Different Equilibrium Positions[a].

geometry	$R_e(S_0)$	BI	$R_e^B(S_1)$	BI	$R_e^{U1}(S_1)$	BI	$R_e^{U2}(S_1)$	BI	$R_e^{U1}(S_2)$	BI	$R_e^{U2}(S_2)$	BI
$R(N^1C^2)$	1.363	1.06	1.363	1.06	1.360	1.06	1.363	1.07	1.357	1.06	1.360	1.06
$R(C^2N^3)$	1.375	1.04	1.375	1.04	1.381	1.05	1.375	1.05	1.379	1.05	1.386	1.01
$R(N^3C^4)$	1.383	1.04	1.383	1.04	1.406	1.04	1.409	1.00	1.363	1.06	1.335	1.15
$R(C^4C^5)$	1.480	1.03	1.480	1.02	1.378	1.37	1.419	1.14	1.371	1.41	1.441	1.10
$R(C^5C^6)$	1.347	1.66	1.347	1.68	1.411	1.24	1.370	1.55	1.493	1.15	1.354	1.68
$R(C^6N^1)$	1.388	1.06	1.388	1.06	1.408	1.09	1.402	1.02	1.382	1.11	1.382	1.08
$R(C^2O)$	1.198	1.59	1.198	1.59	1.200	1.57	1.201	1.58	1.201	1.57	1.195	1.60
$R(C^4O)$	1.198	1.62	1.198	1.63	1.370	1.16	1.380	1.11	1.357	1.16	1.634	0.83
$R(C^5C)$	1.511	1.00	1.514	1.00	1.515	1.01	1.513	1.01	1.503	1.02	1.512	1.01
$R(C^aC)$	1.519	1.01	1.510	1.02	1.517	1.01	1.518	1.01	1.519	1.00	1.517	1.01
$R(C^aC^b)$	1.403	1.25	1.441	1.26	1.404	1.34	1.399	1.37	1.405	1.34	1.403	1.36
$R(C^bC^c)$	1.398	1.30	1.436	1.28	1.390	1.43	1.401	1.37	1.389	1.44	1.392	1.42
$R(C^cC^d)$	1.398	1.24	1.435	1.28	1.402	1.36	1.395	1.40	1.402	1.36	1.400	1.37
$R(C^dC^e)$	1.398	1.27	1.435	1.28	1.390	1.43	1.401	1.37	1.390	1.43	1.392	1.42
$R(C^eC^f)$	1.398	1.30	1.436	1.28	1.399	1.37	1.395	1.40	1.401	1.36	1.398	1.38
$R(C^fC^a)$	1.402	1.23	1.441	1.26	1.381	1.46	1.405	1.33	1.381	1.46	1.383	1.45

Table 2. Vertical excitation energies for the two lowest excited states of 5BU.

	S_1 (eV)	S_2 (eV)
SA-CASSCF(20,14)	4.85	7.92
SA-CASSCF(20,15)	5.02	6.22
MS-CASPT2(20,13)	5.02	6.83
MS-CASPT2(20,14)	4.93	6.28
MRCI(20,14)	5.08	7.12
MRCI (D) (20,14)	5.11	6.90
EOM-CCSD	5.13	5.44
LT-DF-LCC2	4.94	5.07
TDDFT (B3LYP)	4.72	4.91

Table 3a. Internal Bond Coordinates and the Wiberg's bond index (BI) of Different Crossing Point Geometries[a].

geometry	$R_{CI}^{B1}(S_1S_2)$	BI	$R_{CI}^{B2}(S_1S_2)$	BI	$R_{CI}^{U1}(S_1S_2)$	BI	$R_{CI}^{U2}(S_1S_2)$	BI
$R(N^1C^2)$	1.363	1.06	1.364	1.06	1.416	0.98	1.358	1.08
$R(C^2N^3)$	1.375	1.04	1.375	1.04	1.359	1.09	1.404	0.99
$R(N^3C^4)$	1.383	1.04	1.383	1.04	1.434	0.94	1.381	1.11
$R(C^4C^5)$	1.480	1.01	1.481	1.01	1.388	1.32	1.338	1.42
$R(C^5C^6)$	1.347	1.66	1.346	1.66	1.521	1.03	1.496	1.14
$R(C^6N^1)$	1.388	1.05	1.388	1.05	1.333	1.15	1.418	0.93
$R(C^2O)$	1.198	1.59	1.198	1.59	1.192	1.62	1.194	1.60
$R(C^4O)$	1.197	1.63	1.196	1.64	1.251	1.32	1.354	1.02
$R(C^5C)$	1.511	1.01	1.505	1.01	1.521	1.00	1.504	1.02
$R(C^aC)$	1.515	1.01	1.511	1.01	1.520	1.00	1.519	1.01
$R(C^aC^b)$	1.441	1.22	1.452	1.05	1.405	1.33	1.404	1.33
$R(C^bC^c)$	1.440	1.24	1.398	1.36	1.390	1.43	1.390	1.43
$R(C^cC^d)$	1.394	1.35	1.431	1.26	1.402	1.36	1.401	1.36
$R(C^dC^e)$	1.450	1.07	1.430	1.28	1.390	1.43	1.390	1.43
$R(C^eC^f)$	1.447	1.07	1.405	1.33	1.401	1.37	1.399	1.37
$R(C^fC^a)$	1.401	1.32	1.449	1.06	1.382	1.46	1.382	1.47

[a]Bond lengths are given in Å. The labeling of atoms is given in Figure 1.

Table 3b. Internal Bond Coordinates and the Wiberg's bond index (BI) of Different Crossing Point Geometries[a].

geometry	$R_{CI}^{B}(S_0S_1)$	BI	$R_{CI}^{U}(S_0S_1)$	BI
$R(N^1C^2)$	1.368	1.04	1.369	1.06
$R(C^2N^3)$	1.380	1.02	1.404	1.01
$R(N^3C^4)$	1.381	1.05	1.388	1.02
$R(C^4C^5)$	1.481	1.01	1.302	1.44
$R(C^5C^6)$	1.347	1.66	1.514	1.04
$R(C^6N^1)$	1.385	1.05	1.424	0.99

R(C^2O)	1.222	1.56	1.193	1.61
R(C^4O)	1.197	1.63	1.449	0.96
R(C^5C)	1.507	1.02	1.509	1.01
R(C^aC)	1.504	1.01	1.517	1.01
R(C^aC^b)	1.455	1.19	1.404	1.34
R(C^bC^c)	1.462	1.42	1.390	1.43
R(C^cC^d)	1.386	1.47	1.401	1.36
R(C^dC^e)	1.376	1.18	1.391	1.42
R(C^eC^f)	1.462	1.10	1.399	1.37
R(C^fC^a)	1.461	1.10	1.382	1.46

[a]Bond lengths are given in Å. The labeling of atoms is given in Figure 1.

Figure Captions:

Figure 1: The ground state optimized geometry of 5BU. Colors: red for oxygen, blue for nitrogen, gray for carbon and white for hydrogen.

Figure 2: The $R_e^{U1}(S_1)$ optimized geometry of 5BU obtained for the first excited state with changes on the uracil branch.

Figure 3: The $R_e^{U2}(S_1)$ optimized geometry of 5BU obtained for the first excited state with changes on the uracil branch.

Figure 4: The $R_e^{U1}(S_2)$ optimized geometry of 5BU obtained for the second excited state with changes on the uracil branch.

Figure 5: The $R_e^{U2}(S_2)$ optimized geometry of 5BU obtained for the second excited state with changes on the uracil branch.

Figure 6: Laser induced fluorescence spectrum of 5BU.

Figure 7: The global energy diagram of different local minima and conical intersection points on the PES for different excited state levels.

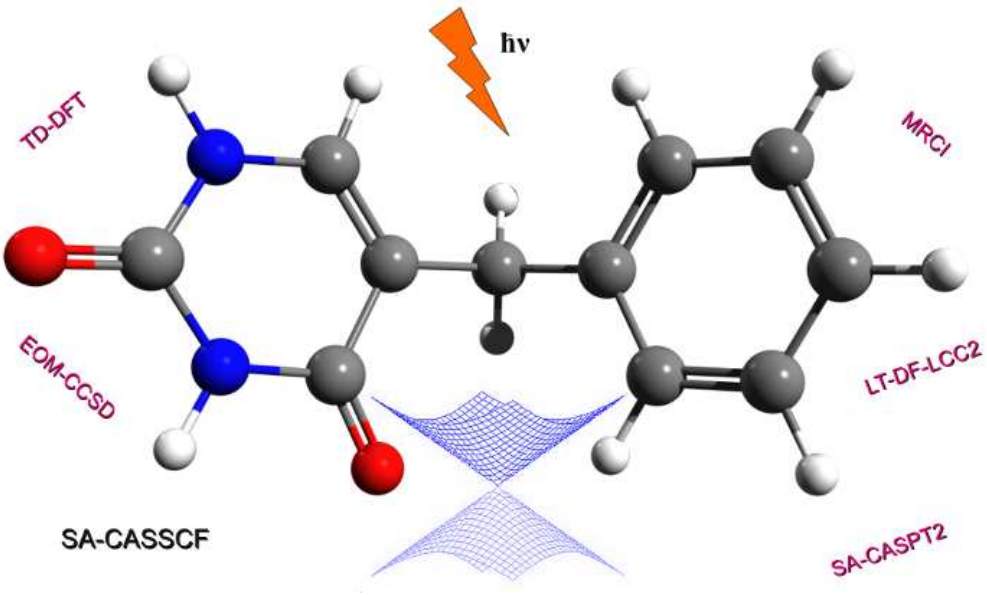

58x34mm (300 x 300 DPI)

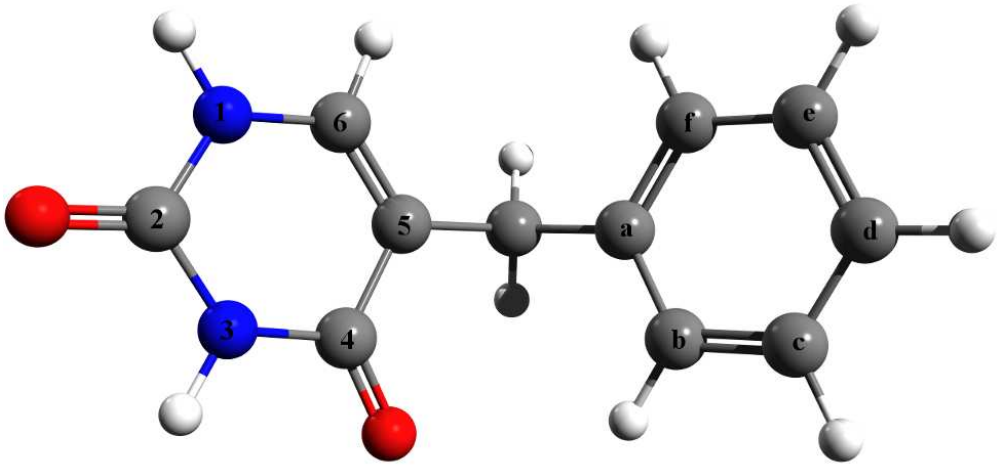

82x40mm (300 x 300 DPI)

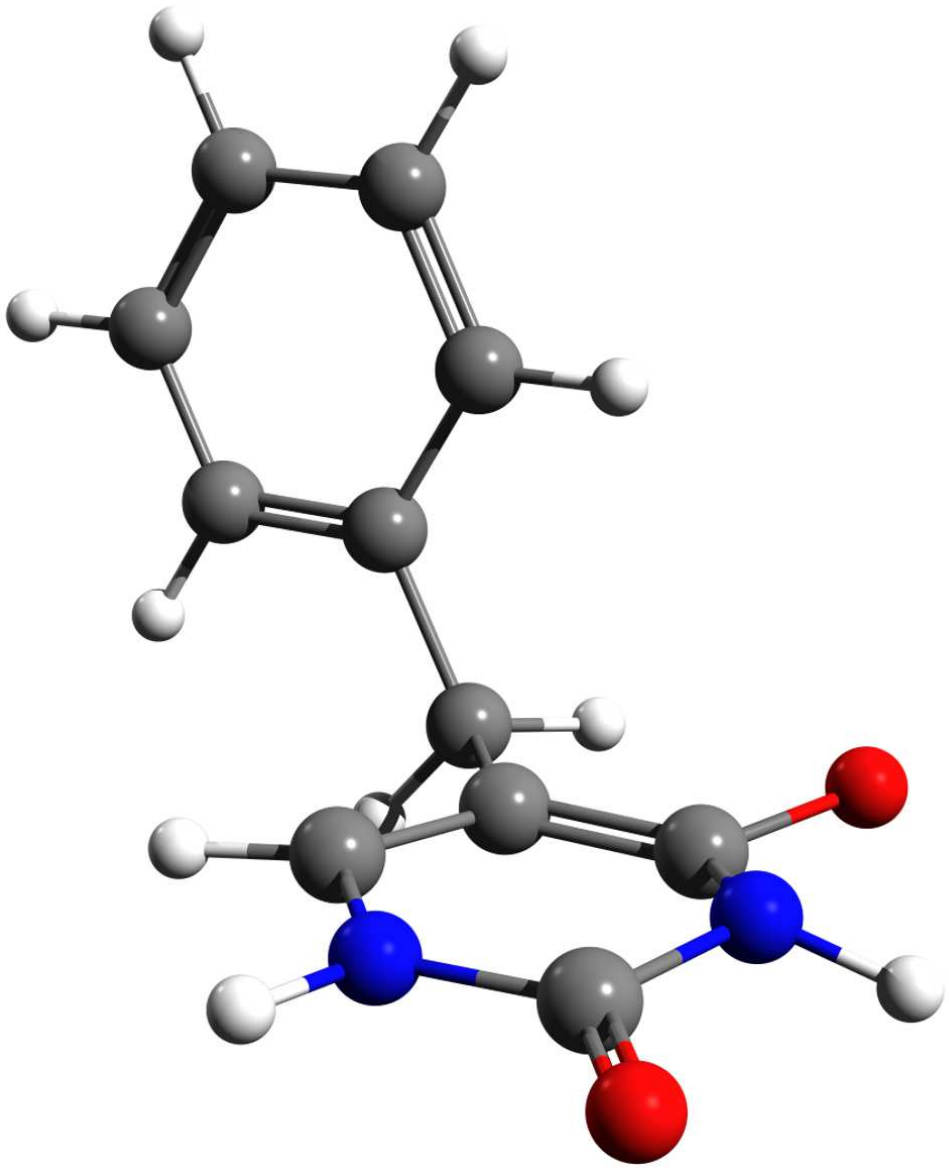

82x100mm (300 x 300 DPI)

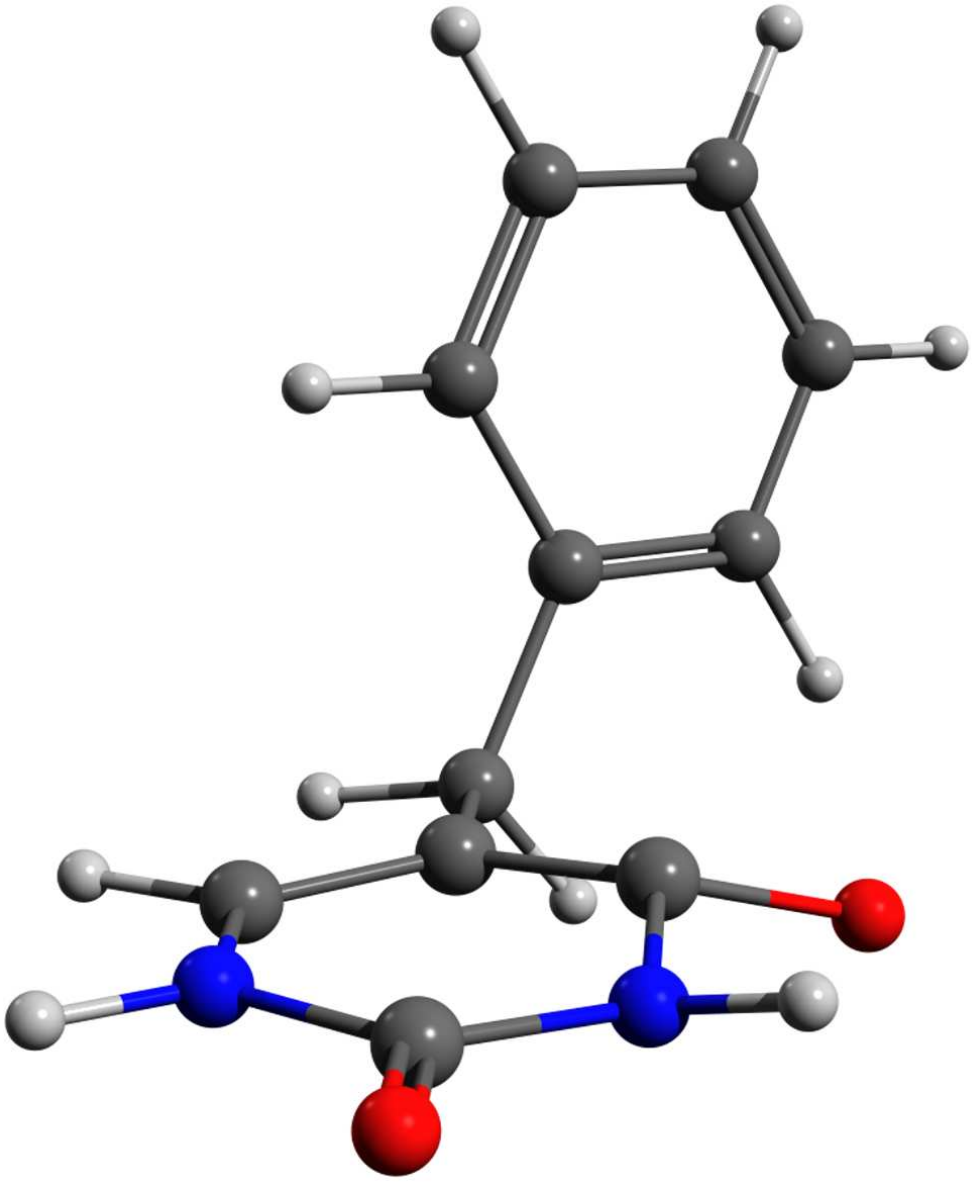

83x100mm (300 x 300 DPI)

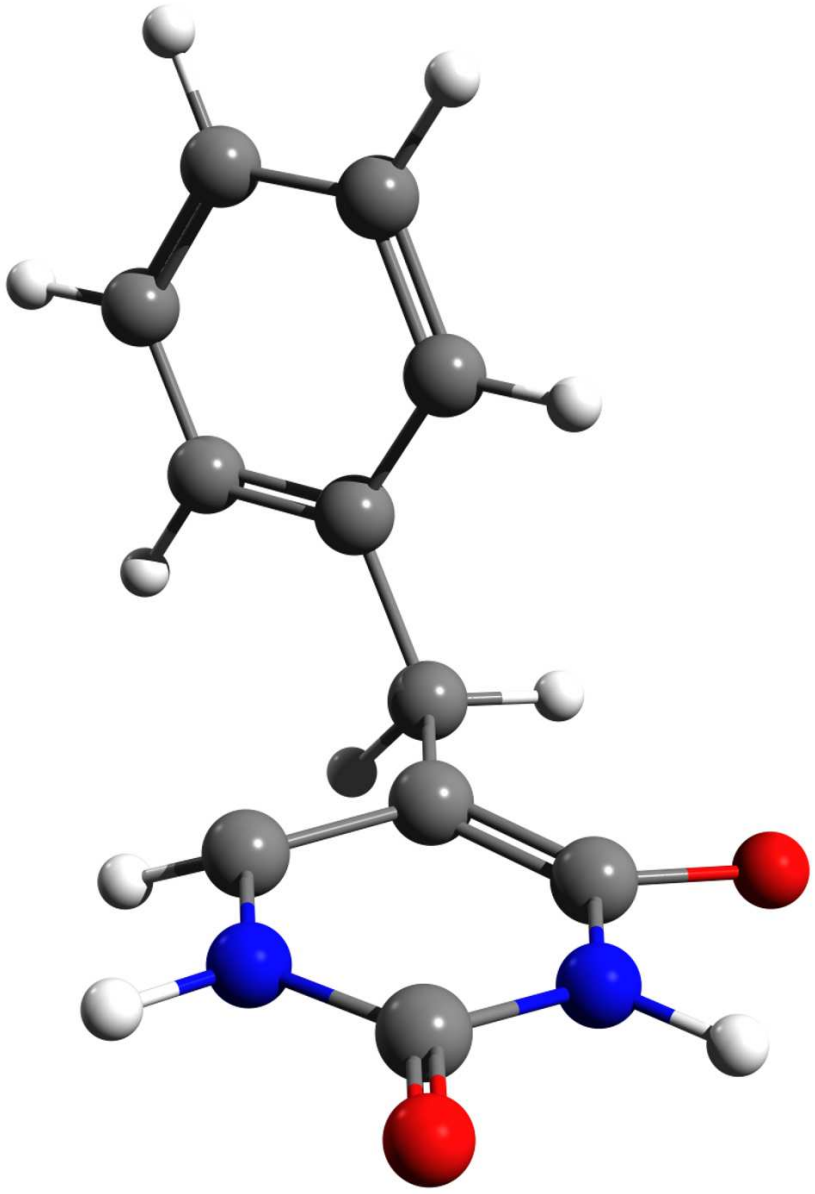

82x117mm (300 x 300 DPI)

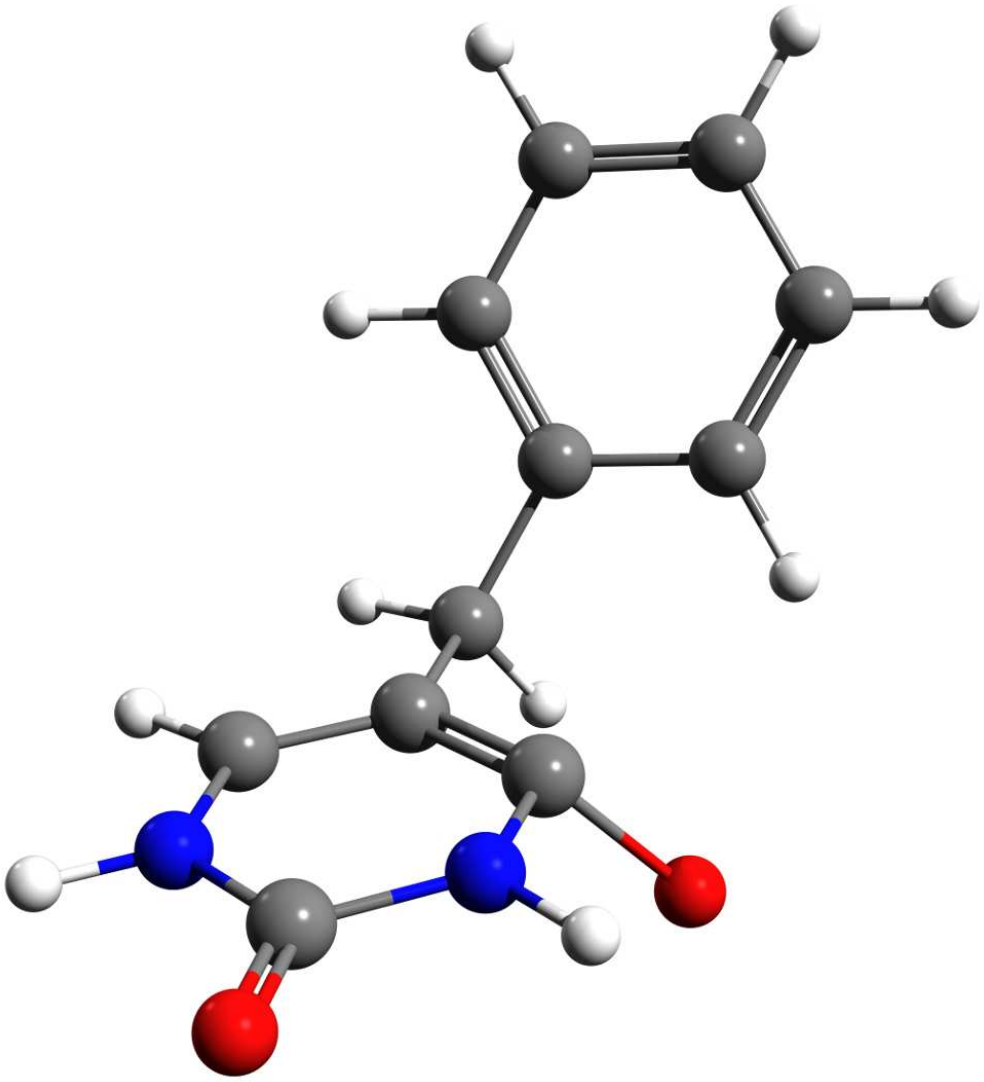

82x90mm (300 x 300 DPI)

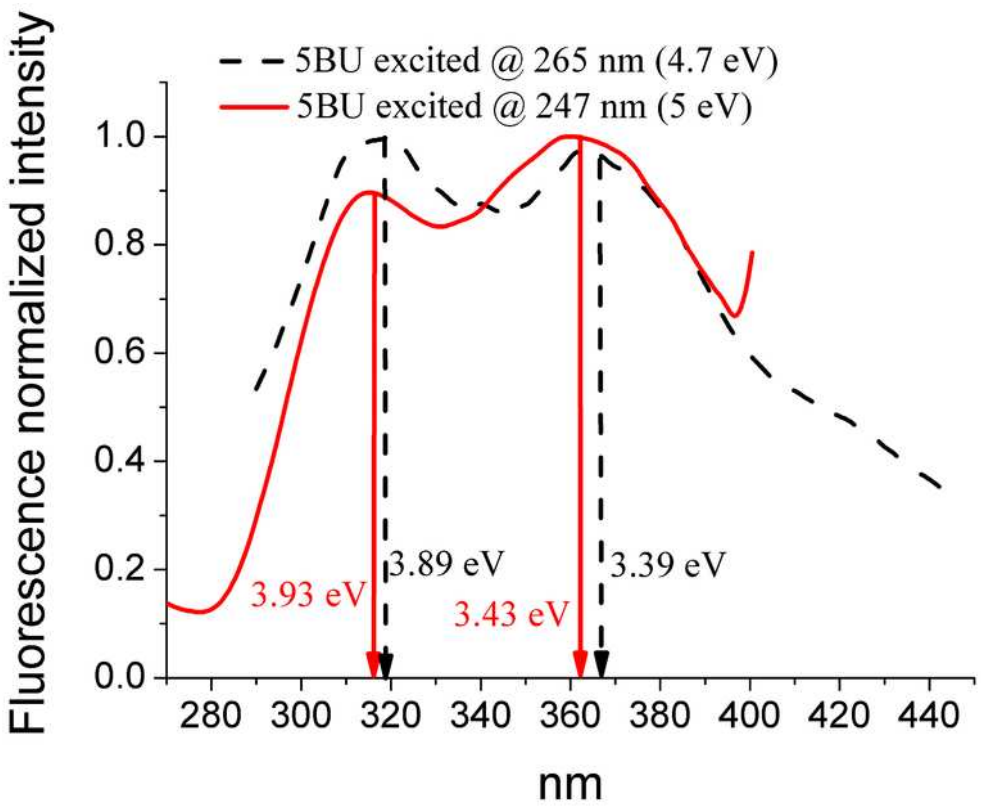

66x52mm (300 x 300 DPI)

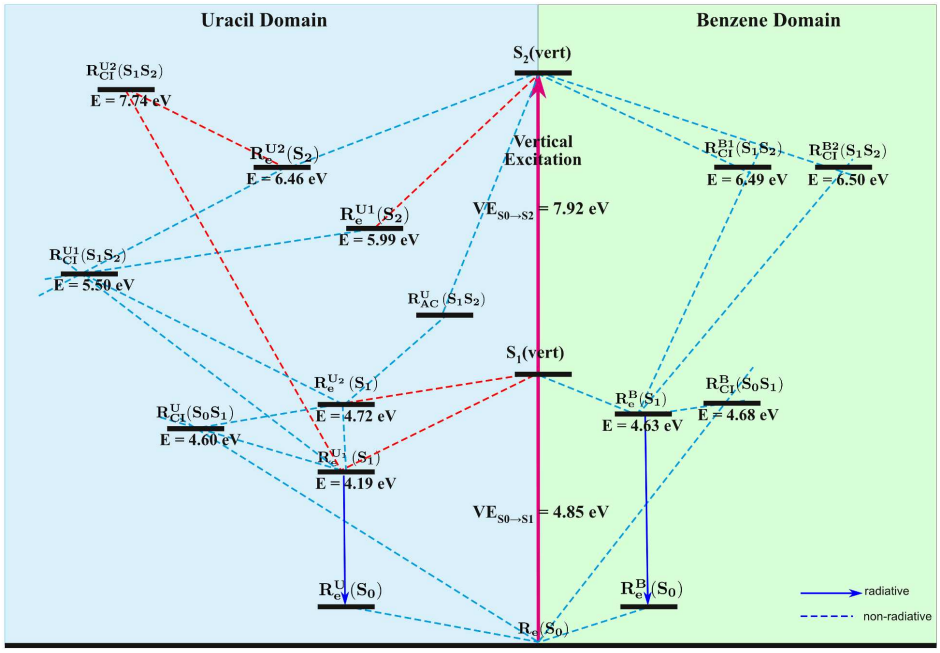

175x123mm (300 x 300 DPI)